Constraining a general $U(1)'$ inverse seesaw model from vacuum stability, dark matter, and collider

Arindam Das,[1,*] Srubabati Goswami,[2,†] Vishnudath K. N.,[2,3,‡] and Takaaki Nomura[4,§]

[1]*Department of Physics, Osaka University, Toyonaka, Osaka 560-0043, Japan*
[2]*Theoretical Physics Division, Physical Research Laboratory, Ahmedabad—380009, India*
[3]*Discipline of Physics, Indian Institute of Technology, Gandhinagar—382355, India*
[4]*School of Physics, KIAS, Seoul 02455, Korea*

(Received 18 May 2019; accepted 2 March 2020; published 20 March 2020)

We consider a class of gauged $U(1)$ extensions of the Standard Model (SM), where the light neutrino masses are generated by an inverse seesaw mechanism. In addition to the three right handed neutrinos, we add three singlet fermions and demand an extra Z_2 symmetry under which, the third generations of both of the neutral fermions are odd, which in turn gives us a stable dark matter candidate. We express the $U(1)$ charges of all the fermions in terms of the $U(1)$ charges of the standard model Higgs and the new complex scalar. We study the bounds on the parameters of the model from vacuum stability, perturbative unitarity, dark matter relic density, and direct detection constraints. We also obtain the collider constraints on the Z' mass and the $U(1)'$ gauge coupling. Finally, we compare all the bounds on the Z' mass versus the $U(1)'$ gauge coupling plane.

DOI: 10.1103/PhysRevD.101.055026

I. INTRODUCTION

The discovery of the Higgs boson with a mass of 125 GeV at the Large Hadron Collider (LHC) [1,2] has placed the Standard Model (SM) on a firm footing. However, the SM still does not have answers to some of the very fundamental questions like the origin of the neutrino masses and the existence of dark matter (DM). A straight forward way to include the generation of the sub-eV scale neutrino masses and the presence of the DM into the SM is by adding extra particles, which may or may not involve the extension of the SM gauge group.

Among the various beyond Standard Model (BSM) scenarios that have been proposed in the literature, the models in which the SM is extended by a $U(1)$ gauge group has received some attention. The models with an extra $U(1)$ gauge group naturally contain three right-handed neutrinos as a result of the conditions for the gauge anomaly cancellation. Thus, the active light neutrino masses can be generated via the canonical type-I seesaw mechanism [3–6]. However, in canonical type-I seesaw model, which is considered in most of the $U(1)$ extended models, one either has to go for extremely large Majorana masses ($\sim 10^{14}$ GeV) or very small Yukawa couplings ($\sim 10^{-6}$), making it difficult to probe the heavy neutrinos at the colliders. Motivated by testability in colliders, various TeV scale extensions of the type-I seesaw model have been considered in the literature (for recent reviews, see [7–10]). One of the most popular TeV scale seesaw models is the inverse seesaw model [11], where the smallness of the neutrino mass can then be attributed to a small lepton number violating term. A tiny value of this lepton number violating term is deemed natural, since when this parameter is zero, the global $U(1)$ lepton number symmetry is reinstated and neutrinos are massless. Especially, an inverse seesaw mechanism in the context of a $U(1)_{B-L}$ extension of the SM has been studied in Ref. [12]. In these models, the presence of extra singlet fermions (in addition to the right-handed neutrinos) helps us to bring down the seesaw scale (which is the $U(1)$ breaking scale) to $\sim O(\text{TeV})$, simultaneously allowing for large Yukawa couplings, $Y_\nu \sim O(0.1)$.

An important aspect of the $U(1)$ extended models which has been scrutinized recently is the implications for the stability of the electroweak (EW) vacuum [13–22]. The measured values of the SM parameters, especially the top mass M_t and strong coupling constant α_s, implies that there exists an extra deeper minima, which threatens the stability of the present EW vacuum [23,24], since this may tunnel into that true vacuum. The calculation of the decay probability suggests that the present EW vacuum is metastable at 3σ which means that the decay time is greater

*arindam.das@het.phys.sci.osaka-u.ac.jp
†sruba@prl.res.in
‡vishnudath@prl.res.in
§nomura@kias.re.kr

than the age of the Universe. It is well known that the scalar couplings pull the vacuum toward stability whereas the Yukawa couplings push it toward instability. The EW vacuum stability in the context of a class of minimal $U(1)$ extensions containing extra scalars and fermions has been studied by the authors of [16–18,20], and they have shown that the behavior of the EW vacuum depends also on the $U(1)$ quantum numbers chosen, since the renormalization group equations (RGEs) depend on these quantum numbers. The conformal symmetric versions of such models have been considered in Refs. [21,22].

As already mentioned, the existence of the DM is another major motivation for going beyond the Standard Model. Measurements by Planck and WMAP demonstrate that nearly 85% of the Universe's matter density is dark [25]. Hence, it is very important to study models that can simultaneously explain neutrino mass as well as DM and their theoretical as well as phenomenological implications. The models with an extra $U(1)$ gauge group can accommodate a DM candidate even in the minimal version (with type-I seesaw), by adding an additional Z_2 symmetry [26,27], where the third generation of the right-handed neutrinos act as the DM candidate. Other versions of the $U(1)_{B-L}$ extension with scalar DM have been studied in [28–31]. Also, there are various realizations of the grand unified theories that predict the existence of extra Z' boson [32,33]. The presence of the extra Z' boson that couples to the quarks and the leptons also gives rise to a rich collider phenomenology in the $U(1)$ models [20,22,34–37]. Searches for such Z' boson through its decay dileptons have been conducted by the ATLAS and CMS Collaborations, and lower limits on the Z' mass have been obtained [38–40].

In this paper, we consider a class of gauged $U(1)$ extensions of the SM, where active light neutrino masses are generated by an inverse seesaw mechanism. In addition to the three right-handed neutrinos, we add three singlet fermions and demand an extra Z_2 symmetry under which, the third generations of both the neutral fermions are odd, which in turn gives us a stable DM candidate. This allows us to consider large neutrino Yukawa couplings and at the same time, keeping the $U(1)'$ symmetry breaking scale to be of the order of $\sim O(1)$ TeV. The main difference of this inverse seesaw model from that considered in [12] is that the extra neutral fermions that we are adding are singlets under the gauge group, and hence we do not have to worry about anomaly cancellation. Also, instead of considering one particular model, we express the $U(1)$ charges of all the fermions in terms of the $U(1)$ charges of the SM Higgs and the new complex scalar. We perform a comprehensive study of the bounds on the model parameters from low energy neutrino data, vacuum stability, perturbative unitarity, and DM, as well as collider constraints. The rest of the paper is organized as follows. In Secs. II and III, we introduce the class of the $U(1)$ models under consideration and discuss the fermionic and the scalar sectors. We discuss the fitting of the neutral fermion mass matrix in Sec. IV by taking all the experimental constraints into account. In Sec. V, we discuss the RGE evolution of the couplings and present the parameter space allowed by vacuum stability and perturbative unitarity in various planes. This is followed by a discussion on the DM scenario in these models, where we present the parameter space giving the correct relic density and satisfying the direct detection bounds at the same time. In Sec. VII, we discuss the combined bounds from vacuum stability, unitarity, DM relic density, and the collider constraints and finally, we summarize in Sec. VIII.

II. MODEL AND NEUTRINO MASS AT THE TREE LEVEL

The model considered is based on the gauge group $SU(3)_c \times SU(2)_L \times U(1)_Y \times U(1)'$. In addition to the SM particles, we have three right-handed neutrinos ν_{Ri}, a complex scalar Φ required to break the $U(1)'$ symmetry, and three gauge singlet Majorana fermions S_i. An extra Z_2 symmetry is imposed to have a stable fermionic dark matter. The matter and Higgs sector field content along with their transformation properties under $SU(3)_c \times SU(2)_L \times U(1)_Y \times U(1)'$ are given below.

$$Q_L = \begin{bmatrix} u_L \\ d_L \end{bmatrix} \sim \left(3, 2, \frac{1}{6}, x_q\right); \qquad d_R \sim \left(3, 1, -\frac{1}{3}, x_d\right);$$
$$u_R \sim \left(3, 1, \frac{2}{3}, x_u\right), \tag{2.1}$$

$$l_L = \begin{bmatrix} \nu_L \\ e_L \end{bmatrix} \sim \left(1, 2, -\frac{1}{2}, x_l\right); \qquad e_R \sim (1, 1, -1, x_e);$$
$$\nu_R \sim (1, 1, 0, x_\nu), \tag{2.2}$$

$$H = \frac{1}{\sqrt{2}} \begin{pmatrix} G^+ \\ v + h + iG^0 \end{pmatrix} \sim \left(1, 2, \frac{1}{2}, \frac{x_H}{2}\right);$$
$$\Phi = \frac{1}{\sqrt{2}}(\phi + u + i\chi) \sim (1, 1, 0, -x_\Phi), \tag{2.3}$$

$$S \sim (1, 1, 0, 0). \tag{2.4}$$

Note that the generation indices have been suppressed here. Under Z_2, the third generation of ν_R and S, i.e., ν_{R3} and S_3 are odd, whereas all the other particles are even and we assume that this Z_2 is not broken.

The $U(1)'$ charges of the fermions are defined to satisfy the gauge and gravitational anomaly-free conditions,

$$
\begin{aligned}
U(1)' \times [SU(3)_c]^2 &: 2x_q - x_u - x_d = 0,\\
U(1)' \times [SU(2)_L]^2 &: 3x_q + x_l = 0,\\
U(1)' \times [U(1)_Y]^2 &: x_q - 8x_u - 2x_d + 3x_l - 6x_e = 0,\\
[U(1)']^2 \times U(1)_Y &: x_q^2 - 2x_u^2 + x_d^2 - x_l^2 + x_e^2 = 0,\\
[U(1)']^3 &: 6x_q^3 - 3x_u^3 - 3x_d^3 + 2x_l^3 - x_\nu^3 - x_e^3 = 0,\\
U(1)' \times [\mathrm{grav}]^2 &: 6x_q - 3x_u - 3x_d + 2x_l - x_\nu - x_e = 0. \quad (2.5)
\end{aligned}
$$

The most general Yukawa Lagrangian (along with the Majorana mass for S) invariant under $SU(3)_c \times SU(2)_L \times U(1)_Y \times U(1)'$ that could be written using the fields given above is

$$
\begin{aligned}
-L_{\mathrm{Yukawa}} = {} & Y_e \bar{l}_L H e_R + Y_\nu \bar{l}_L \tilde{H} \nu_R + Y_u \bar{Q}_L \tilde{H} u_R + Y_d \bar{Q}_L H d_R \\
& + y_{NS} \bar{\nu}_R \Phi S + \frac{1}{2} \overline{S^c} M_\mu S + \mathrm{H.c.}, \quad (2.6)
\end{aligned}
$$

where $\tilde{H} = i\sigma_2 H^*$. The invariance of this Yukawa Lagrangian under the $U(1)'$ symmetry gives us the following conditions:

$$
\frac{x_H}{2} = -x_q + x_u = x_q - x_d = -x_l + x_\nu = x_l - x_e; \quad -x_\Phi = x_\nu. \quad (2.7)
$$

Using these conditions and the anomaly-free conditions, the $U(1)'$ charges of all the fermions could be determined in terms of x_H and x_Φ as

$$
\begin{aligned}
& x_\nu = -x_\Phi, \qquad x_l = -x_\Phi - \frac{x_H}{2}, \qquad x_e = -x_\Phi - x_H,\\
& x_q = \frac{1}{6}(2x_\Phi + x_H), \qquad x_u = \frac{1}{3}(2x_H + x_\Phi),\\
& x_d = \frac{1}{3}(x_\Phi - x_H). \quad (2.8)
\end{aligned}
$$

Note that the choice $x_\Phi = 1$ and $x_H = 0$ correspond to the well-known $U(1)_{B-L}$ model. From Eq. (2.6), after symmetry breaking, the terms relevant for neutrino mass are

$$
-L_{\mathrm{mass}} = \bar{\nu}_L M_D \nu_R + \overline{\nu_R} M_R S + \frac{1}{2} \overline{S^c} M_\mu S + \mathrm{H.c.}, \quad (2.9)
$$

where $M_D = Y_\nu \langle H \rangle$ and $M_R = y_{NS} \langle \Phi \rangle$. The neutral fermion mass matrix M_ν can be defined as

$$
-L_{\mathrm{mass}} = \frac{1}{2} (\overline{\nu_L^c} \bar{\nu}_R \overline{S^c}) \begin{pmatrix} 0 & M_D^* & 0 \\ M_D^\dagger & 0 & M_R \\ 0 & M_R^T & M_\mu \end{pmatrix} \begin{pmatrix} \nu_L \\ \nu_R^c \\ S \end{pmatrix} + \mathrm{H.c.}. \quad (2.10)
$$

The mass scales of the three submatrices of M_ν may naturally have a hierarchy $M_R \gg M_D \gg M_\mu$. Then, the effective light neutrino mass matrix in the seesaw approximation is given by

$$
M_{\mathrm{light}} = M_D^* (M_R^T)^{-1} M_\mu M_R^{-1} M_D^\dagger. \quad (2.11)
$$

Because of the extra Z_2 symmetry, the Yukawa coupling matrices Y_ν and y_{NS} and hence the mass matrices M_D and M_R will have the following textures:

$$
M_R = y_{NS} \langle \Phi \rangle \sim \begin{pmatrix} \times & \times & 0 \\ \times & \times & 0 \\ 0 & 0 & \times \end{pmatrix} \quad \text{and}
$$

$$
M_D = Y_\nu \langle H \rangle \sim \begin{pmatrix} \times & \times & 0 \\ \times & \times & 0 \\ \times & \times & 0 \end{pmatrix}. \quad (2.12)
$$

In addition, we will choose M_μ to be diagonal without loss of generality. Since ν_{R3} and S_3 do not mix with other neutral fermions, they will not contribute to the seesaw mechanism and we will have a minimal inverse seesaw mechanism ($3\,\nu_L + 2\,\nu_R + 2\,\mathrm{S}$ case) in which the lightest active neutrino will be massless. The two fermions ν_{R3} and S_3 mix among themselves and the lightest mass eigenstate could be a stable DM candidate. In the heavy sector, we will have two pairs of degenerate pseudo-Dirac neutrinos of masses of the order $\sim M_R \pm M_\mu$ that mix with the active light neutrinos. Thus, we have an inverse seesaw mechanism in which the smallness of M_{light} is naturally attributed to the smallness of both M_μ and $\frac{M_D}{M_R}$. For instance, $M_{\mathrm{light}} \sim \mathcal{O}(0.1)$ eV can easily be achieved by taking $\frac{M_D}{M_R} \sim 10^{-2}$ and $M_\mu \sim \mathcal{O}(1)$ keV. Thus, the seesaw scale can be lowered down considerably for typical values of the parameters—$Y_\nu \sim \mathcal{O}(0.1)$, $M_D \sim 10$ GeV, and $M_R \sim 1$ TeV.

III. SCALAR POTENTIAL OF THE MODEL AND SYMMETRY BREAKING

The scalar potential of the model is given by

$$
\begin{aligned}
V(\Phi, H) = {} & m_1^2 H^\dagger H + \lambda_1 (H^\dagger H)^2 + \lambda_3 H^\dagger H \Phi^\dagger \Phi \\
& + m_2^2 \Phi^\dagger \Phi + \lambda_2 (\Phi^\dagger \Phi)^2. \quad (3.1)
\end{aligned}
$$

The trivial conditions that give a stable potential are

$$
\lambda_1 > 0, \qquad \lambda_2 > 0 \quad \text{and} \quad \lambda_3 > 0, \quad (3.2)
$$

and if $\lambda_3 < 0$, the stability of the potential can still be achieved by satisfying the following conditions:

$$
\lambda_1 > 0, \qquad \lambda_2 > 0, \qquad 4\lambda_1 \lambda_2 - \lambda_3^2 > 0. \quad (3.3)
$$

The above conditions are obtained by demanding the Hessian matrix corresponding to the potential to be positive definite at large field values [16,41,42].

The two scalar fields acquire vacuum expectation values ($vevs$) given by

$$\langle H\rangle = \frac{1}{\sqrt{2}}\begin{pmatrix}0\\ v\end{pmatrix}, \qquad \langle \Phi\rangle = \frac{u}{\sqrt{2}}. \tag{3.4}$$

The values of v and u are determined by the minimization conditions and are given by

$$v^2 = \frac{m_2^2\lambda_3/2 - m_1^2\lambda_2}{\lambda_1\lambda_2 - \lambda_3^2/4}, \qquad u^2 = \frac{m_1^2\lambda_3/2 - m_2^2\lambda_1}{\lambda_1\lambda_2 - \lambda_3^2/4}. \tag{3.5}$$

After symmetry breaking, the mixing between the fields h and ϕ could be rotated away by an orthogonal transformation to get the physical mass eigenstates as

$$\begin{pmatrix}h_1\\ h_2\end{pmatrix} = \begin{pmatrix}\cos\theta & -\sin\theta\\ \sin\theta & \cos\theta\end{pmatrix}\begin{pmatrix}h\\ \phi\end{pmatrix}. \tag{3.6}$$

The masses of the scalar eigenstates are

$$m_{h_{1,2}}^2 = \lambda_1 v^2 + \lambda_2 u^2 \mp \sqrt{(\lambda_1 v^2 - \lambda_2 u^2)^2 + (\lambda_3 uv)^2}. \tag{3.7}$$

From these, one can get the relations

$$\begin{aligned}\lambda_1 &= \frac{m_{h_1}^2}{4v^2}(1+\cos 2\theta) + \frac{m_{h_2}^2}{4v^2}(1-\cos 2\theta),\\ \lambda_2 &= \frac{m_{h_1}^2}{4u^2}(1-\cos 2\theta) + \frac{m_{h_2}^2}{4u^2}(1+\cos 2\theta),\\ \lambda_3 &= \sin 2\theta\left(\frac{m_{h_2}^2 - m_{h_1}^2}{2uv}\right).\end{aligned} \tag{3.8}$$

We use these equations to set the initial conditions on the scalar couplings λ_1, λ_2, and λ_3 while running the renormalization group equations. Also, from the above equations, one can get

$$\tan 2\theta = \frac{\lambda_3 uv}{\lambda_1 v^2 - \lambda_2 u^2}. \tag{3.9}$$

A. Perturbative unitarity

In addition to the vacuum stability conditions, the constraints from the perturbative unitarity conditions also put bounds on the model parameters. By considering the $hh \to hh$ and $\phi\phi \to \phi\phi$ processes, one can derive combined constraints on the three couplings appearing in the scalar potential [43,44],

$$|\lambda_3| \le 8\pi; \quad 3(\lambda_1+\lambda_2) \pm \sqrt{\lambda_3^2 + 9(\lambda_1-\lambda_2)^2} \le 8\pi. \tag{3.10}$$

Demanding the other running couplings to remain in the perturbative regime gives us

$$g_i \le \sqrt{4\pi}, \tag{3.11}$$

where g_i stands for SM gauge couplings. For the $U(1)$ gauge coupling g', we require

$$(x_{q,d,u,l,e,\nu,\Phi})g', \qquad (x_H/2)g' < \sqrt{4\pi}. \tag{3.12}$$

IV. NUMERICAL ANALYSIS AND PARAMETER SCANNING IN THE NEUTRINO SECTOR

To study the parameter space allowed by vacuum stability as well as perturbativity bounds up to $M_{\rm Planck}$ using the RGEs, we have to first fix the initial values for all the couplings. While setting the initial values for the neutrino Yukawa couplings Y_ν and y_{NS}, we have to make sure that they reproduce the correct oscillation parameters and satisfy all the experimental constraints. To do this, we find sample benchmark points for Y_ν, y_{NS}, and M_μ and the vev of the extra scalar $\Phi(u)$ by fitting them with all the constraints using the downhill simplex method [45]. Note that here, Y_ν is a complex 3×2 matrix, y_{NS} is a complex 2×2 matrix, and M_μ is a 2×2 diagonal matrix with real entries. The various constraints we have taken are as follows:

(i) Cosmological constraint on the sum of light neutrino masses as given by the Planck 2018 results [46]. This puts an upper limit on the sum of active light neutrino masses to be

$$\Sigma = m_1 + m_2 + m_3 < 0.14 \text{ eV}. \tag{4.1}$$

Note that in our case, the lightest active neutrino is massless and also we are restricting our analysis only to the normal hierarchy (NH) of the active neutrino masses since the vacuum stability, dark matter, and collider analyses are independent of the hierarchy of the light neutrino masses. In addition, it has been found that the best fit of the data is for the NH and IH is disfavored with a $\Delta\chi^2 = 4.7(9.3)$ without (with) Super-Kamiokande atmospheric neutrino data [47]. Thus, we have

$$m_1 = 0, \quad m_2 = \sqrt{\Delta m_{\rm sol}{}^2}, \quad m_3 = \sqrt{\Delta m_{atm}^2}. \tag{4.2}$$

(ii) The constraints on the oscillation parameters in their 3σ range, given by the global analysis [48,49] of neutrino oscillation data with three light active neutrinos following NH, are given in Table I. We use the standard parametrization of the Pontecorvo–Maki–Nakagawa–Sakata (PMNS) matrix in which

TABLE I. The oscillation parameters in their 3σ range for the normal hierarchy (NH) as given by the global analysis of neutrino oscillation data with three light active neutrinos [48].

Parameter	$3-\sigma$ range in NH
$\Delta m^2_{\rm sol}/10^{-5}$ eV^2	$6.80 \to 8.02$
$\Delta m^2_{\rm atm}/10^{-3}$ eV^2	$+2.399 \to +2.593$
$\sin^2\theta_{12}$	$0.272 \to 0.346$
$\sin^2\theta_{23}$	$0.418 \to 0.613$
$\sin^2\theta_{13}$	$0.01981 \to 0.02436$

TABLE II. Two sample benchmark points for the neutrino sector. The above parameters give the correct mixing angles and satisfy the nonunitarity constraints on $U_{\rm PMNS}$. The value of $\mathrm{Br}(\mu \to e\gamma)$ is given as a check.

Parameter	BM-I	BM-II
$\mathrm{Tr}[Y_\nu Y_\nu^\dagger]$	0.0898	0.4000
$[Y_\nu]_{3\times 2}$	$\begin{pmatrix} 0.0694 - i0.1182 & 0 - i0.0499 \\ 0.0038 - i0.0022 & 0.0778 + i0.0442 \\ -0.0008 - i0.2183 & -0.0071 - i0.1128 \end{pmatrix}$	$\begin{pmatrix} -0.0210 + i0.2269 & -0.0329 + i0.0036 \\ 0.0495 - i0.0352 & -0.2321 - i0.3021 \\ -0.1081 - i0.3771 & 0.1450 + i0.1526 \end{pmatrix}$
$\mathrm{Tr}[y_{NS} Y_R^\dagger]$	0.0101	0.1472
$[y_{NS}]_{2\times 2}$	$\begin{pmatrix} 0.0031 - i0.0082 & 0.0375 - i0.0351 \\ 0.0821 + i0.0093 & -0.0002 - i0.0241 \end{pmatrix}$	$\begin{pmatrix} 0.2861 + i0.0073 & -0.0025 + i0.1521 \\ 0.0623 - i0.0545 & -0.1596 - i0.0990 \end{pmatrix}$
$[M_\mu]_{2\times 2}$ GeV	$\begin{pmatrix} 1.0921 \times 10^{-6} & 0 \\ 0 & -2.2092 \times 10^{-8} \end{pmatrix}$	$\begin{pmatrix} 1.2655 \times 10^{-8} & 0 \\ 0 & -2.5248 \times 10^{-8} \end{pmatrix}$
M_j GeV	1766.82, 1766.82, 3085.87, 3085.87	2227.88, 2227.88, 3659.58, 3659.58
$\mathrm{Br}(\mu \to e\gamma)$	4.0946×10^{-13}	2.2954×10^{-13}
u (TeV)	50	12

$$U_\nu = \begin{pmatrix} c_{12}c_{13} & s_{12}c_{13} & s_{13}e^{-i\delta} \\ -c_{23}s_{12} - s_{23}s_{13}c_{12}e^{i\delta} & c_{23}c_{12} - s_{23}s_{13}s_{12}e^{i\delta} & s_{23}c_{13} \\ s_{23}s_{12} - c_{23}s_{13}c_{12}e^{i\delta} & -s_{23}c_{12} - c_{23}s_{13}s_{12}e^{i\delta} & c_{23}c_{13} \end{pmatrix} P, \tag{4.3}$$

where $c_{ij} = \cos\theta_{ij}$, $s_{ij} = \sin\theta_{ij}$, and the phase matrix $P = \mathrm{diag}(1, e^{i\alpha_2}, e^{i(\alpha_3+\delta)})$ contains the Majorana phases.

(iii) The constraints on the nonunitarity of $U_{PMNS} = U_L$ as given by the analysis of electroweak precision observables along with various other low energy precision observables [50]. At 90% confidence level, we have

$$|U_L U_L^\dagger| = \begin{pmatrix} 0.9979\text{–}0.9998 & <10^{-5} & <0.0021 \\ <10^{-5} & 0.9996\text{–}1.0 & <0.0008 \\ <0.0021 & <0.0008 & 0.9947\text{–}1.0 \end{pmatrix}. \tag{4.4}$$

This also takes care of the constraints coming from various charged lepton flavor violating decays like $l_i \to l_j\gamma$. For example, the branching ratio for the decay $\mu \to e\gamma$ is constrained as [51]

$$\mathrm{Br}(\mu \to e\gamma) < 4.2 \times 10^{-13}. \tag{4.5}$$

In addition, it has been shown in Ref. [52] that the $\mu \to e$ conversion in nuclei can give the strongest bound out of all the flavor violating observables in the case of type-I seesaw models. The bound on the branching ratio for the $\mu \to e$ conversion in Gold (Au) nucleus reads as [53]

$$\mathrm{Br}(\mu\,\mathrm{Au} \to \mathrm{e}\,\mathrm{Au}) < 7 \times 10^{-3}. \tag{4.6}$$

This has been converted into a bound on the parameter $\hat{R}_{e\mu}$ in Ref. [52] as

$$\hat{R}_{e\mu} < 9.7 \times 10^{-6}, \tag{4.7}$$

where

$$\hat{R}_{e\mu} = 2\sum_j (Y_\nu)^*_{ej}(Y_\nu)_{\mu j}\left(\frac{m_W^2}{M_j^2}\right)\mathrm{Log}\left(\frac{M_j}{m_W}\right), \tag{4.8}$$

where $j = 1, 2$, M_1, M_2 are the heavy neutrino masses such that $M_1 \neq M_2$ and the factor of 2 takes care of the degeneracy in mass spectrum. In our fitting, we have made sure that the parameter sets that we consider satisfy all these bounds.

In Table II, we give two benchmark points consistent with all the experimental data discussed above. As a consistency check, we also give the value of $\mathrm{Br}(\mu \to e\gamma)$ obtained at the two benchmark points.

V. RGE EVOLUTION

The couplings in any quantum field theory get corrections from higher-order loop diagrams and as a result, the couplings run with the renormalization scale. We have the renormalization group equation (RGE) for a coupling C as

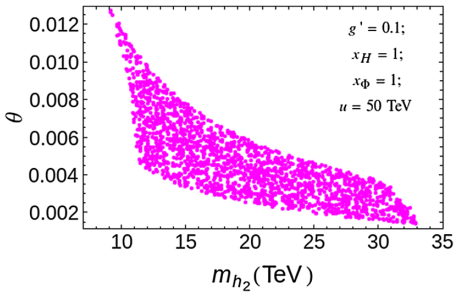

FIG. 1. Region in the $m_{h_2} - \theta$ plane allowed by both vacuum stability and perturbativity bounds up to M_{Planck} for the model with $x_H = x_\Phi = 1$. For the neutrino Yukawa couplings, we have used BM-I from the Table II and we have fixed $g' = 0.1$ and $y_{NS}^{33} = 0.5$.

$$\mu \frac{dC}{d\mu} = \sum_i \frac{\beta_C^{(i)}}{(16\pi^2)^i}, \tag{5.1}$$

where i stands for the ith loop and β_C is the corresponding β function.

We have evaluated the SM coupling constants at the top quark mass scale and then run them using the RGEs from M_t to M_{Planck}. For this, we have taken into account the various threshold corrections at M_t [54–56]. Then the SM RGEs are used to run all the couplings up to the vev of the new scalar, after which, the new couplings enter. The modified RGEs for the $SU(3)_c \times SU(2)_L \times U(1)_Y \times U(1)'$ have been used. These have been generated using SARAH [57]. Since we have considered only the one-loop RGEs of all the required parameters, it has to be noted that the allowed parameter space that we present is minimal. The inclusion of the higher-order RG effects will increase the size of the allowed parameter space.[1] The RGEs that we have used are given in the Appendix. Throughout this paper, we have fixed the standard model parameters as $m_h = 125.6$ GeV, $M_t = 173.4$ GeV, and $\alpha_s = 0.1184$. Also, we have kept the $U(1)$ gauge mixing to be 0 at the scale u throughout this paper.

Figure 1 displays the allowed region in the $m_{h_2} - \theta$ plane for the model with $x_H = x_\Phi = 1$, keeping all the other parameters fixed. For the neutrino Yukawa couplings, we have used BM-I from Table II and we have fixed $g' = 0.1$ and $y_{NS}^{33} = 0.5$. From the figure, one can see that for higher values of θ, only smaller values of m_{h_2} are allowed whereas for smaller values of θ, larger values of m_{h_2} over a wider range are allowed. Also, it can be seen that for this model with the considered set of parameters, the values of $m_{h_2} > 33$ TeV and $\theta > 0.012$ are disallowed.

[1]The effect of the two-loop RGEs with one-loop matching is discussed in Ref. [18] in the context of a class of minimal $U(1)$ extensions of the SM.

In Fig. 2, we have plotted the running of λ_1, λ_2, and λ_3 for the model with $x_H = x_\Phi = 1$ for two different values of m_{h_2} and θ. The figure in the left side is for $m_{h_2} = 15$ TeV and $\theta = 0.004$, whereas the one in the right side is for $m_{h_2} = 20$ TeV and $\theta = 0.003$. For the neutrino Yukawa couplings, we have used BM-I from Table II and we have fixed $g' = 0.1$ and $y_{NS}^{33} = 0.5$. We can see that all the three quartic couplings remain positive up to M_{Planck} for both the cases implying that the electroweak vacuum is absolutely stable. This can be seen from Fig. 1 as well where the above-mentioned points fall in the stable region. Here, the presence of the extra scalar coupling helps in stabilizing the vacuum.

In Fig. 3, we have plotted the regions allowed by both vacuum stability and perturbativity bounds up to M_{Planck} in the $m_{h_2} - x_H$ and $m_{h_2} - x_\Phi$ planes, for two different values of θ. The red regions are for $\theta = 0.003$ and the blue regions are for $\theta = 0.01$. Figure 3(a) shows the allowed regions in the $m_{h_2} - x_H$ plane keeping all the other parameters fixed. For the neutrino Yukawa couplings, we have used BM-I from Table II and we have fixed $x_\Phi = 1$, $g' = 0.1$, and $y_{NS}^{33} = 0.5$. It can be seen that for $\theta = 0.01$, a very narrow region of m_{h_2} in the range $\approx$10–11.7 TeV is allowed by the stability and perturbativity constraints and the corresponding allowed range of x_H is ≈ -5.6–4.1. Here, the higher values of m_{h_2} are disfavored by the perturbativity constraints, whereas the lower values of m_{h_2} are disfavored by the constraints from vacuum stability. At the same time, for $\theta = 0.003$, $m_{h_2} \approx$ 11–30 TeV is allowed depending on the value of x_H.

Similarly, in Fig. 3(b), we have shown the allowed region in the $m_{h_2} - x_\Phi$ plane keeping $x_H = 1$ and all the other parameters fixed for two different values of θ. Here also, for $\theta = 0.01$, the values of m_{h_2} greater than 11.7 TeV are disfavored by unitarity constraints. The lower values of m_{h_2} are disfavored by the stability constraints depending on the value of x_Φ. For $-1.6 \leq x_\Phi \leq 1.6$, values of m_{h_2} less than $\sim$10 TeV are disallowed, whereas for $-5 \leq x_\Phi \leq -3$ and $3 \leq x_\Phi \leq 4$, values of m_{h_2} as low as $\sim$4 TeV are allowed. For $\theta = 0.003$, values of $m_{h_2} <$ 13.4–15.8 TeV are disallowed depending on the values of x_H, but values as high as 30 TeV are allowed for $-5 \leq x_H \leq 4$. These results are consistent with the observations from Fig. 1 where we have seen that for $x_H = x_\Phi = 1$, larger(smaller) values of m_{h_2} are disfavored for larger(smaller) values of θ.

In Fig. 4, we have presented the regions in the $x_\Phi - x_H$ plane allowed by both vacuum stability and perturbativity up to M_{Planck} for fixed values of m_{h_2}, θ, and g'. For the neutrino Yukawa couplings, we have used the BM-I in Table II and we have taken $y_{NS}^{33} = 0.5$. The mass of the extra scalar has been taken to be 6 TeV (10 TeV) in the left (right) panel and the values of θ and g' are taken to be 0.01 and 0.1, respectively, for both the plots. From these two figures, we can see that increasing the scalar mass will

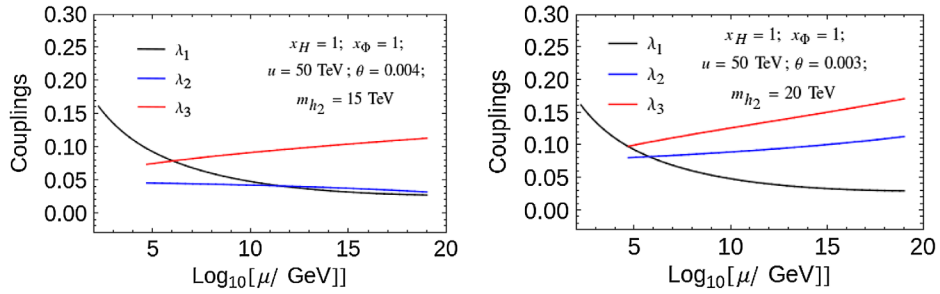

(a) $m_{h_2} = 15$ TeV, $\theta = 0.004$ (b) $m_{h_2} = 20$ TeV, $\theta = 0.003$

FIG. 2. Running of λ_1, λ_2, and λ_3 for the model with $x_H = x_\Phi = 1$ for two different values of m_{h_2} and θ. For the neutrino Yukawa couplings, we have used BM-I from Table II and we have fixed $g' = 0.1$ and $y_{NS}^{33} = 0.5$.

allow more values of x_Φ for a given value of x_H. In fact, one can see that the allowed values for x_Φ lie in the ranges $\approx \pm 2.7$ to ± 6 and $\approx \pm 1$ to ± 6 for the figures in the left and the right panels, respectively. Also, x_H lies in the range ≈ -6.8 to 7 for both the cases with the considered values of the parameters. This can be understood from Eq. (3.8) which shows that higher value of m_{h_2} implies higher value of the scalar couplings which in turn favors stability.

Figure 5 displays the regions allowed by both vacuum stability and perturbativity up to $M_{\rm Planck}$ in the $M_{Z'} - x_H$ plane for fixed values of m_{h_2}, θ, and x_Φ. Here also, we have used the BM-I in Table II for the neutrino Yukawa couplings and we have taken $y_{NS}^{33} = 0.5$. The mass of the extra scalar has been taken to be 7 and 10.5 TeV in the

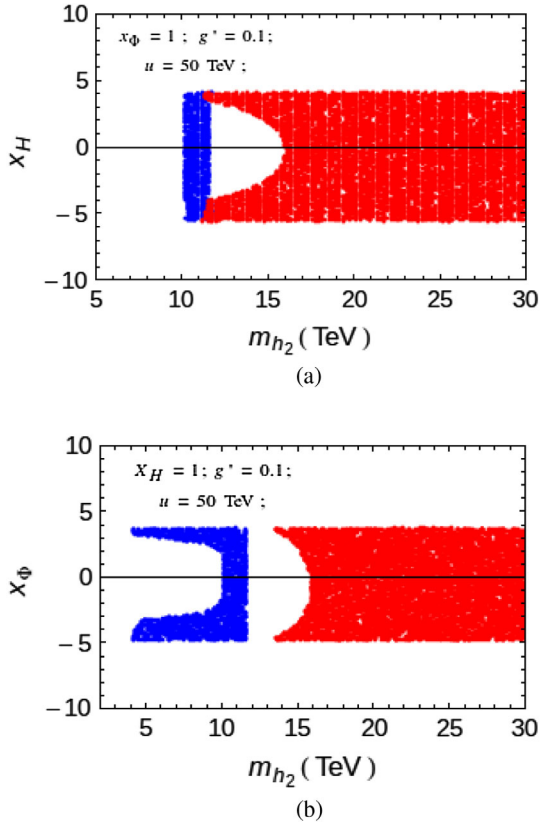

(a)

(b)

FIG. 3. Regions in the $m_{h_2} - x_H$ and $m_{h_2} - x_\Phi$ planes allowed by both vacuum stability and perturbativity bounds up to $M_{\rm Planck}$ for two different values of θ. For the left panel, we have fixed $x_\Phi = 1$ and for the right panel, we have fixed $x_H = 1$. For the neutrino Yukawa couplings, we have used BM-I from Table II and we have fixed $g' = 0.1$ and $y_{NS}^{33} = 0.5$. The red region is for $\theta = 0.003$ and the blue region is for $\theta = 0.01$.

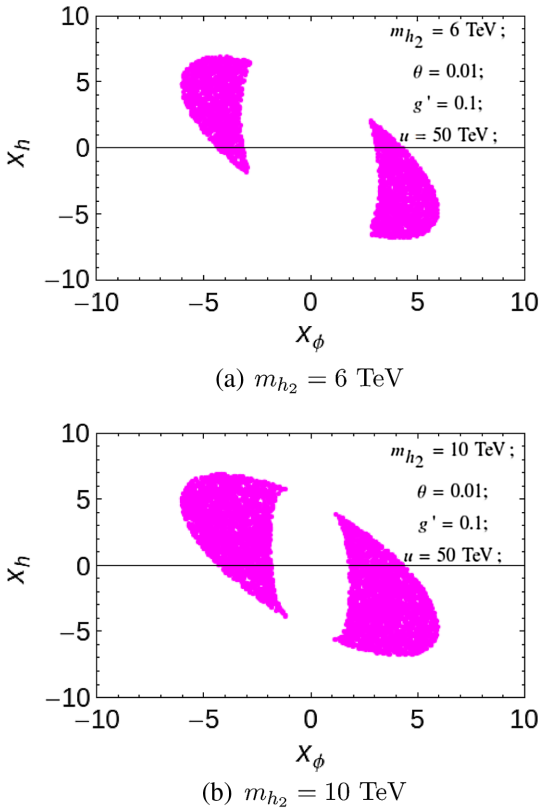

(a) $m_{h_2} = 6$ TeV

(b) $m_{h_2} = 10$ TeV

FIG. 4. Regions in the $x_\Phi - x_H$ plane allowed by both vacuum stability and perturbativity up to $M_{\rm Planck}$. We have taken the mass of the extra scalar to be 6 TeV (10 TeV) in the left (right) panel. For the neutrino Yukawa couplings, we have used BM-I from Table II and we have fixed $\theta = 0.01$, $g' = 0.1$, and $y_{NS}^{33} = 0.5$ for both the plots.

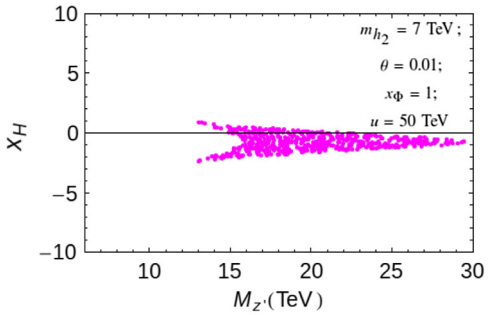

(a) $m_{h_2} = 7$ TeV

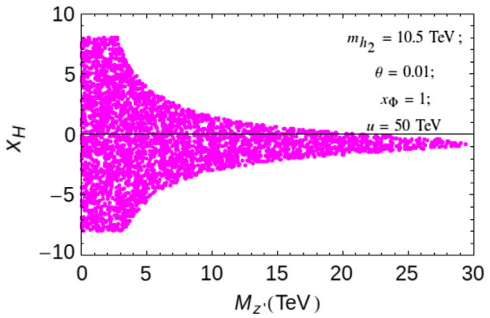

(b) $m_{h_2} = 10.5$ TeV

FIG. 5. Regions in the $M_{Z'} - x_H$ plane allowed by both vacuum stability and perturbativity bounds up to M_{Planck}. We have taken the mass of the extra scalar to be 7 TeV (10.5 TeV) in the left (right) panel. For the neutrino Yukawa couplings, we have used BM-I from Table II and we have fixed $\theta = 0.01$, $x_\Phi = 1$, and $y_{NS}^{33} = 0.5$ for both the plots.

left and the right panels, respectively, and the values of θ and x_Φ are taken to be 0.01 and 1 for both the plots. Also, we have varied g' from 0 to 1 keeping u fixed at 50 TeV and x_H in the range -8 to 8. The corresponding values of $M_{Z'}$ have been calculated using

$$M_{Z'} = \sqrt{(x_\Phi g' u)^2 + \left(\frac{x_H}{2} g' v_{\text{SM}}\right)^2}. \tag{5.2}$$

From these figures, we can see that lower values of $M_{Z'}$ allow large values of x_H (or, equivalently lower values of g'). Also, one can note that for a lower scalar mass, the lower values of M_Z' (or equivalently, lower values of g') are disfavored. For $m_{h_2} = 7$ TeV, values of $M_{Z'}$ less than 13 TeV are disallowed and a very small range of x_H is allowed, whereas for $m_{h_2} = 10.5$ TeV, values of $M_{Z'}$ as low as 100 GeV are allowed and correspondingly, x_H is allowed from -8 to 8.

VI. DARK MATTER SCENARIO

In this section, we discuss dark matter physics in our model with respect to the constraints from relic density and direct detection experiments. As mentioned earlier, the third generations of N_R and S_L (N_R^3, S_L^3) are odd under the Z_2 parity in the general $U(1)'$ inverse seesaw model that we consider. This ensures the stability of N_R^3 and S_L^3 which is required for these to be potential DM candidates. As a result, the relevant interactions in the Lagrangian can be written as

$$-\mathcal{L}^2_{\text{mass}} \supset y_{NS}^{33} \overline{N_R^3} S_L^3 \Phi + M_S^{33} \overline{S_L^{3c}} S_L^3. \tag{6.1}$$

Note that N_R^3 cannot couple to the SM Higgs and lepton doublets due to the Z_2 symmetry. After the symmetry breaking, we have $\langle \Phi \rangle = \frac{u}{\sqrt{2}}$ and the mass matrix can be written as

$$M_{N^3 S^3} = \begin{pmatrix} 0 & M_{NS}^{33} \\ M_{NS}^{33} & M_S^{33} \end{pmatrix}, \tag{6.2}$$

where $M_{NS}^{33} = \frac{y_{NS}^{33} u}{\sqrt{2}}$. Now, rotating the basis we can write the physical eigenstates as

$$\begin{pmatrix} N_R^{3c} \\ S_L^3 \end{pmatrix} = \begin{pmatrix} \cos\bar{\theta} & \sin\bar{\theta} \\ -\sin\bar{\theta} & \cos\bar{\theta} \end{pmatrix} \begin{pmatrix} \psi_1 \\ \psi_2 \end{pmatrix}, \tag{6.3}$$

where $\tan 2\bar{\theta} = |\frac{2M_{NS}^{33}}{-M_S^{33}}| = \sqrt{2}\frac{y_{NS}^{33} u}{M_S^{33}}$. Note that ψ_1 and ψ_2 are Majorana fermions. The mass eigenvalues are obtained as

$$m_{\psi_1,\psi_2} = \frac{1}{2}\sqrt{(M_S^{33})^2 + 4(M_{NS}^{33})^2} \mp \frac{1}{2} M_S^{33}, \tag{6.4}$$

where we take $m_{\psi_1} < m_{\psi_2}$. Thus, ψ_1 is the lightest Z_2 odd particle and our DM candidate. Putting ψ_1 and ψ_2 back into Eq. (6.1) along with the physical mass eigenstates of h and ϕ, we write the interaction among Z_2 odd fermion and scalars as

$$\begin{aligned} -\mathcal{L} \supset\ & y_{NS}^{33}(-\sin\theta\cos\bar{\theta}\cos\bar{\theta} h_1 + \cos\theta\sin\bar{\theta}\sin\bar{\theta} h_2) \\ & \times (-\overline{\psi_1^c}\psi_1 + \overline{\psi_2^c}\psi_2). \end{aligned} \tag{6.5}$$

Then the DM candidate can annihilate through the scalar portal [Fig. 6(a)], where interactions between h_2 and SM particles are induced by scalar mixing [see Eq. (3.6)], and these couplings are equal to the SM Higgs couplings times $\sin\theta$. In addition, the DM can annihilate to the SM particles via Z' exchange [Fig. 6(c)] where the gauge interactions are given by

$$\begin{aligned} \mathcal{L} \supset\ & -\frac{x_\Phi g'}{2} Z'_\mu(\cos^2\bar{\theta}\bar{\psi}_1\gamma^\mu\gamma_5\psi_1 + \sin^2\bar{\theta}\bar{\psi}_2\gamma^\mu\gamma_5\psi_2 \\ & - 2\cos\bar{\theta}\sin\bar{\theta}\bar{\psi}_1\gamma^\mu\gamma_5\psi_2). \end{aligned} \tag{6.6}$$

Furthermore, DM can annihilate into $Z'Z'$ mode via scalar portal where the relevant scalar-$Z'Z'$ interaction is given by

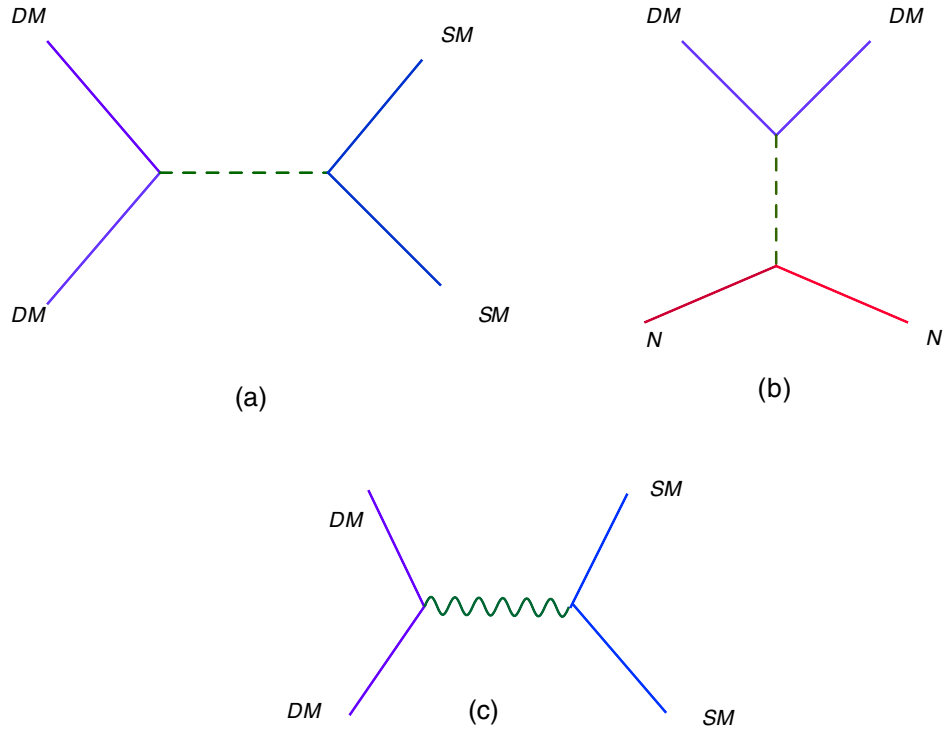

FIG. 6. (a) Scalar mediated DM annihilation, (b) direct detection, and (c) Z' mediated DM annihilation.

$$\mathcal{L} \supset \frac{M_{Z'}^2}{u}\cos\theta h_2 Z'Z' - \frac{M_{Z'}^2}{u}\sin\theta h_1 Z'Z'. \quad (6.7)$$

A. Relic density

Here we analyze the relic density of our DM candidate. The DM candidate ψ_1 annihilates into the SM particles via processes induced by Z' and scalar boson interactions as shown in Fig. 6. Then we estimate the relic density using *micrOMEGAs 4.3.5* [58] implementing the relevant interactions. First, we focus on the parameter space where the Z' mediated process dominates for DM annihilation. For illustration, in Fig. 7, we show the relic density as a function of DM mass ($M_{\rm DM} \equiv m_{\psi_1}$) for $m_{Z'} = 4$ TeV, fixing the other parameters as indicated in the plot. The plot indicates that the required gauge coupling is $g' \gtrsim 0.5$, but it is excluded by the LHC data as we will see later. Note that in this case, the value of g' that gives the correct relic density depends on the choice of x_H and x_Φ since the interaction strength of Z' with the other particles is a product of g' and a linear combination of x_H and x_Φ. If we increase x_H and x_Φ, then the value of g' that can give the correct relic density can be lowered. However, for smaller values of g', the LHC constraints imply much lower values of M'_Z where the Z' exchange is not a dominant process. We also find that the Z' mediated process cannot provide sufficient annihilation cross section to explain the observed relic density if DM is heavier than ∼3 TeV, complying with the requirement that the gauge coupling satisfy $(x_{q,d,u,l,e,\nu,\Phi})g'$, $(x_H/2)g' < \sqrt{4\pi}$ for perturbativity. This tendency comes from the fact that the annihilation cross section is P wave suppressed since our DM is Majorana fermion.

We will now focus on the contribution of h_2 exchange process to the relic density of DM. For illustrating the effect of this process, we show the relic density as a function of DM mass for different values of y_{NS}^{33} and m_{h_2} in Fig. 8. In the left panel, we have fixed $y_{NS}^{33} = 2.5$ and plotted the relic density as a function of $M_{\rm DM}$ for three different values of

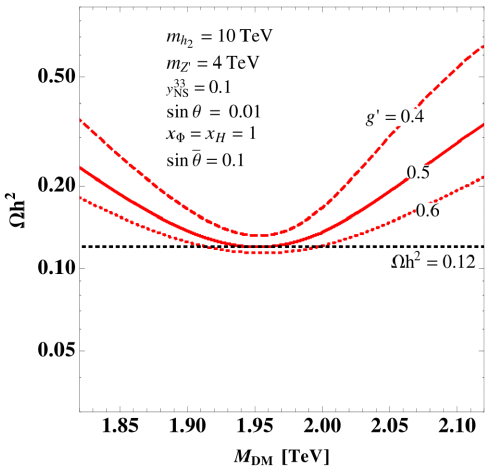

FIG. 7. Relic abundance as a function of DM mass for different values of g'. All the other parameters have been fixed as given in the plot.

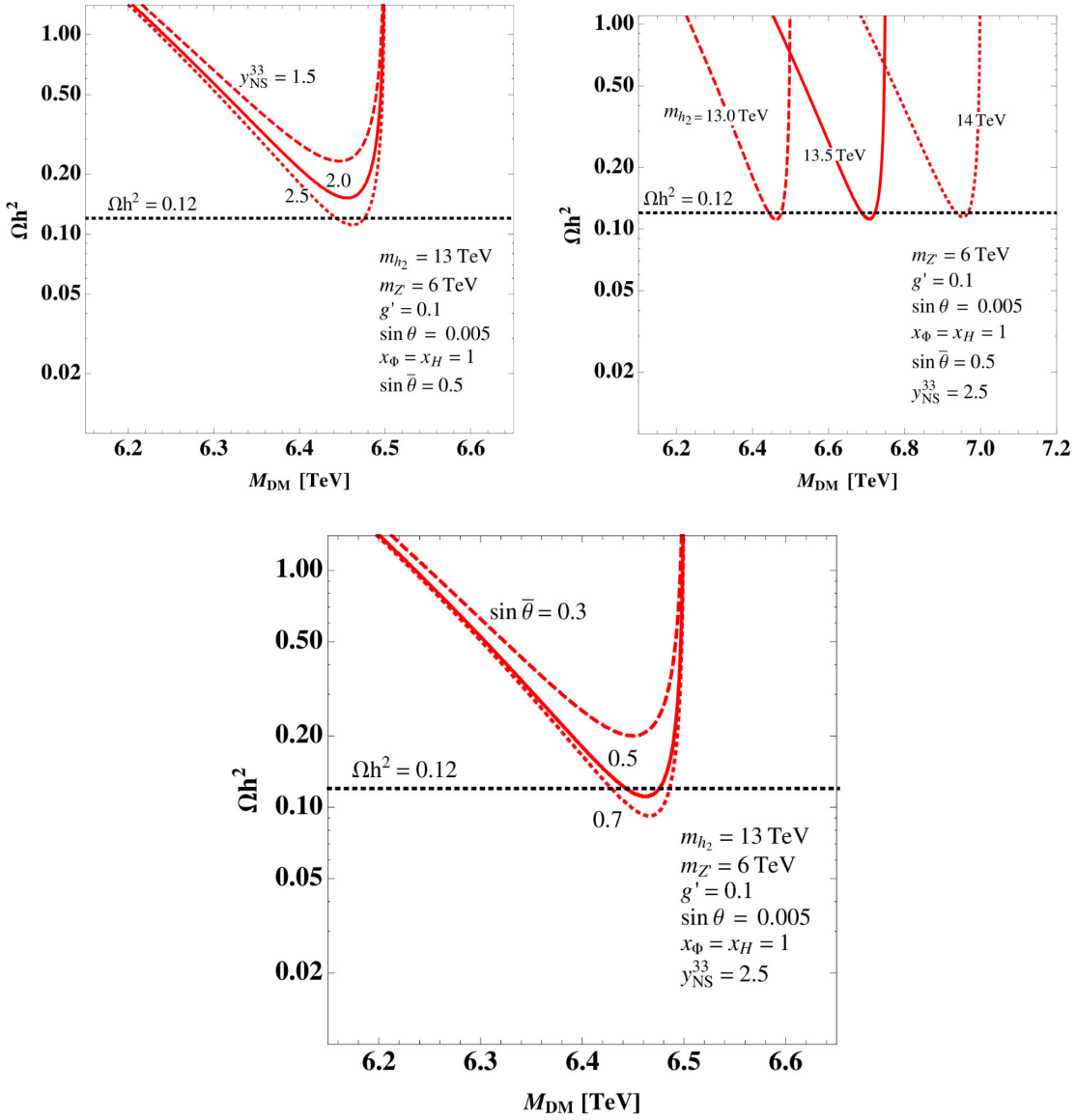

FIG. 8. Relic abundance as a function of DM mass: for different values of y^{33}_{NS} and fixed $m_{h_2} = 13$ TeV (upper left panel); for different values of m_{h_2} and fixed $y^{33}_{NS} = 2.5$ (upper right panel) and for different $\sin\bar{\theta}$ (lower panel).

m_{h_2}, keeping all the other parameters fixed. Similarly, we have taken $m_{h_2} = 13$ TeV in the right plot and plotted the relic density for three different values of y^{33}_{NS}. We have also shown the $\sin\bar{\theta}$ dependence in the lower panel of the same figure. We find that the observed relic density can be realized for $y^{33}_{NS} \gtrsim 2$ when $m_{h_2} = 13$ TeV. In addition, $m_{h_2} \sim 2M_{\rm DM}$ is preferred to enhance the annihilation cross section which implies that m_{h_2} mass is around $\mathcal{O}(10)$ TeV in our model. Note that such a heavy mass scale for h_2 is also preferred in stabilizing the scalar potential as we discussed in the previous section.

We perform a parameter scan and search for the allowed regions which can explain the relic density of DM. First, we perform parameter scan in the following ranges focusing on the scalar exchange process:

$$\begin{aligned} &M_{\rm DM} \in [1.0, 10.0]\ \text{TeV}, \qquad m_{h_2} \in [1.8M_{\rm DM}, 2.2M_{\rm DM}], \\ &y^{33}_{NS} \in [0.2, 3.0], \qquad \sin\theta \in [0.001, 0.02], \\ &x_H \in [-5, 5], \qquad x_\Phi \in [-5, 5], \qquad \sin\bar{\theta} \in [0.2, 0.7], \\ &m_{Z'} = 5\ \text{TeV}, \qquad g' = 0.01. \end{aligned} \tag{6.8}$$

We fixed Z' mass and g' for simplicity. Note that we chose $m_{h_2} \sim 2M_{\rm DM}$ since we can obtain the observed relic density in this region via h_2 exchange process as discussed above. In Fig. 9, we show the allowed parameter space in $M_{\rm DM} - y^{33}_{NS}$ and $m_{h_2} - \sin\theta$ planes that give the correct relic density of DM, $0.11 < \Omega h^2 < 0.13$, adopting the approximate range around the best fit value [46]. From the left panel of Fig. 9, we can see that in general, for larger

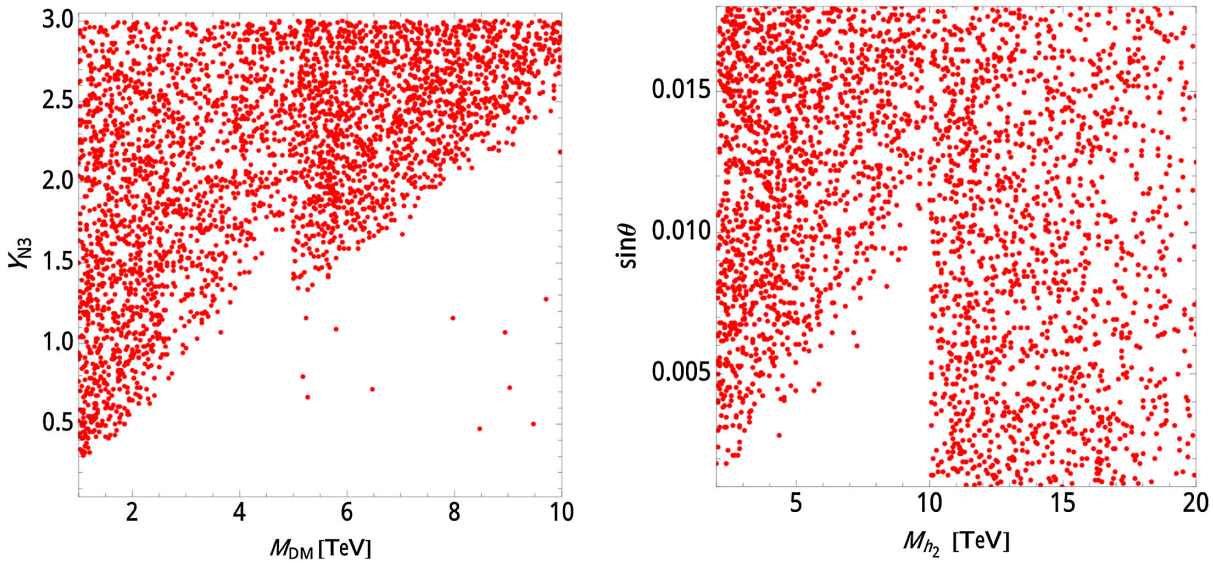

FIG. 9. Parameter regions that give the correct relic density of DM in $M_{\rm DM} - y_{NS}^{33}$ and $M_{h_2} - \sin\theta$ planes for scanning done in the ranges of parameters as given by Eq. (6.8).

values of $M_{\rm DM}$, the allowed values of y_{NS}^{33} are large. But, a few points with smaller values of y_{NS}^{33} are also obtained for $M_{\rm DM} > M_{Z'}$ since $\psi_1\psi_1 \to h_2 \to Z'Z'$ process is kinematically allowed there. In the right panel of Fig. 9, we have shown the allowed parameter space in the $m_{h_2} - \sin\theta$ plane. From this plot, we can see that $\sin\theta$ can be small for $M_{\rm DM} > M_{Z'}$ ($m_{h_2} \sim 2M_{\rm DM}$) since $h_2Z'Z'$ coupling is not suppressed by $\sin\theta$ as we can see from Eq. (6.7). However, we have some lower limit of $\sin\theta$ for $M_{\rm DM} < m_{Z'}$, since here $\psi_1\psi_1 \to h_2 \to Z'Z'$ process is kinematically disallowed and the coupling of h_2 to the SM particles is suppressed by $\sin\theta$.

B. Direct detection

Here we briefly discuss the constraints from the direct detection experiments estimating the DM-nucleon (N) scattering in our model. First, note that the Z' exchange process between DM and nucleon will not get stringent constraint since DM-Z' interaction is via axial vector current due to the Majorana property of DM and provides spin-dependent operator for DM-nucleon interaction. We thus focus on the scalar mediated processes for DM-nucleon scattering where the corresponding Feynman diagram is given in Fig. 6(b). In our case, the DM interacts with the nucleon through the scalar boson exchange (h_1, h_2). The relevant interaction Lagrangian with the mixing effect is given by

$$\begin{aligned}\mathcal{L} \supset\ & C_{\psi_1\psi_1h_1}h_1\overline{\psi_1^c}\psi_1 + C_{\psi_1\psi_1h_1}h_2\overline{\psi_1^c}\psi_1 \\ & + C_{NNh_1}h_1\bar{N}N + C_{NNh_2}h_2\bar{N}N, \end{aligned} \tag{6.9}$$

where the effective couplings are

$$\begin{aligned} C_{\psi_1\psi_1h_1} &= \sin\bar{\theta}\cos\bar{\theta}\cos\theta\frac{y_{NS}^{33}}{\sqrt{2}}, \\ C_{\psi_1\psi_1h_2} &= -\sin\bar{\theta}\cos\bar{\theta}\sin\theta\frac{y_{NS}^{33}}{\sqrt{2}}, \end{aligned} \tag{6.10}$$

$$C_{NNh_1} = \sin\theta g_{hNN}, \qquad C_{NNh_2} = \cos\theta g_{hNN}. \tag{6.11}$$

Hence, the effective Lagrangian can be written as

$$\mathcal{L}_{\rm eff} = G_h\overline{\psi_1}\psi_1\bar{N}N, \tag{6.12}$$

$$G_h = \left[\frac{C_{\psi_1\psi_1h_1}C_{h_1NN}}{m_{h_1}^2} + \frac{C_{\psi_2\psi_2h_2}C_{h_2NN}}{m_{h_2}^2}\right], \tag{6.13}$$

where m_{h_1} and m_{h_2} are the SM and BSM Higgs masses. The corresponding cross section of Fig. 6(b) in the non-relativistic limit can be calculated as

$$\sigma = g_{hNN}^2\frac{M_{\rm DM}^2M_N^2}{16\pi(M_{\rm DM}^2+M_N^2)^2}(y_{NS}^{33}\sin2\bar{\theta}\sin2\theta)^2\left(\frac{1}{m_{h_1}^2}-\frac{1}{m_{h_2}^2}\right)^2, \tag{6.14}$$

where $M_{\rm DM}$ and M_N are the DM and nucleon masses, respectively. The effective coupling can be written as $g_{hNN} = \frac{f_NM_N}{v\sqrt{2}}$, where we apply $f_N = 0.287$ for neutron [59][2] and $v = 246$ GeV. We then estimate the cross sections applying allowed parameter sets obtained in previous subsection, and the results are shown in Fig. 10. The black dotted and dashed lines show the current upper bounds from

[2] f_N for proton has similar value and we here just use f_N in estimating the cross section.

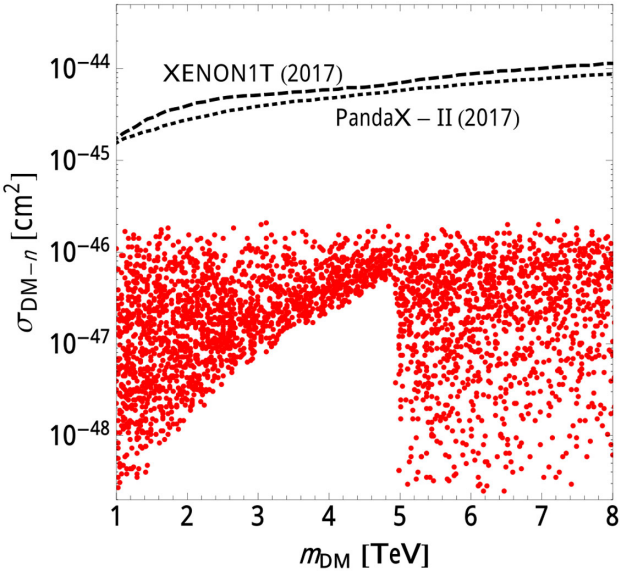

FIG. 10. Nucleon-DM scattering cross section as a function of DM mass for parameters that give the correct relic density. The current upper bounds from PANDAX-II [60] (black dotted line) and XENON-1t [61] (back dashed line) are also shown.

PANDAX-II [60] and XENON-1t [61], respectively. We find that our parameter region is allowed by the direct detection constraints since the cross section is suppressed by small $\sin\theta$, which is also preferred by the constraints from vacuum stability. The cross section will be further explored by the future direct detection experiments like XENON 1t, PandaX, etc.

VII. BOUNDS ON THE $M'_Z - g'$ PLANE

In this section, we consider the production of Z' from the proton proton collision at the LHC and its decay into different types of leptons. We first calculate the Z' production cross section at the LHC from protons followed by the decay into lepton, $pp \to Z' \to \ell^+\ell^-$ with $\ell = e, \mu$. In our analysis, we calculate the cross section combining the electron and muon final states. We compare our cross section with the latest ATLAS search [40] for the heavy Z' resonance. Since we are considering $U(1)'$ models with extra Z', the ATLAS results can be compared directly with our results. Atlas analysis has considered different models like sequential Standard Model (SSM) and Z'_ψ [62], where the Z' decays into e and μ. Conservatively considering these limits for our case, we first produce the Z' (300 GeV $\leq M'_Z \leq$ 6 TeV) at the 13 TeV LHC followed by the decay into the dilepton mode and finally compare with the cross sections in our model. To calculate the bounds on the g', we calculate the model cross section, σ_{Model}, for the process $pp \to Z' \to 2e, 2\mu$, with a $U(1)'$ coupling constant g_{Model} at the LHC at the 13 TeV center of mass energy. Then we compare this with the observed ATLAS bound $(\sigma^{\text{Observed}}_{\text{ATLAS}})$ for $\frac{\Gamma}{m} = 3\%$ which has been studied for the

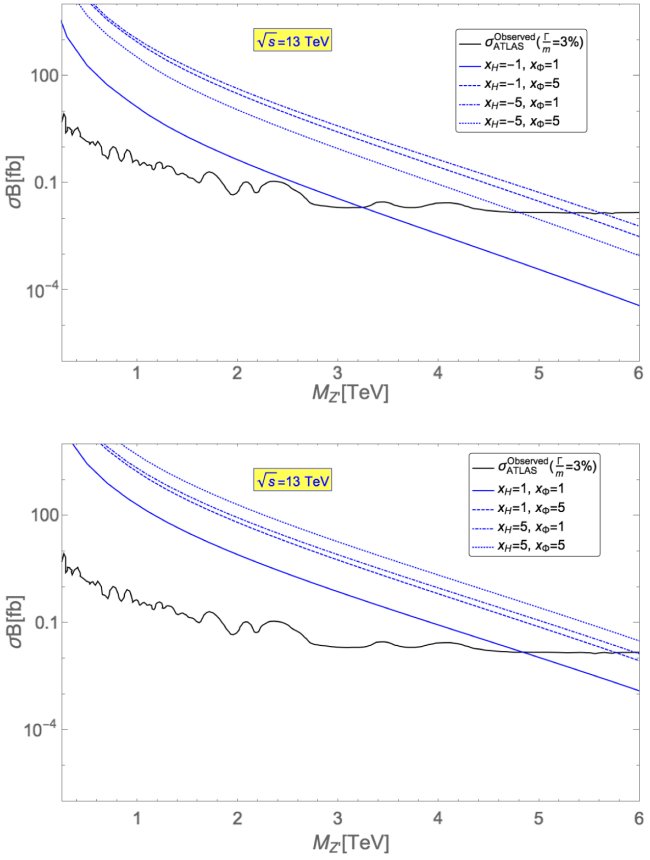

FIG. 11. Comparison between the ATLAS [40] (black solid line) result and model cross sections (blue lines) for the different values of x_H and x_Φ. The model cross sections are produced with $g_{\text{Model}} = 0.05$. The left and right panels correspond to $x_H < 0$ and $x_H > 0$, respectively, and we have considered $x_\Phi > 0$ for both the cases.

SSM. The corresponding cross sections are plotted in Fig. 11 for different choices of x_H and x_Φ. Thus, the value of g' corresponding to a given $M_{Z'}$ is given as

$$g' = \sqrt{\frac{\sigma^{\text{Observed}}_{\text{ATLAS}}}{\left(\frac{\sigma_{\text{Model}}}{g^2_{\text{Model}}}\right)}}, \tag{7.1}$$

since the cross section varies with the square of the $U(1)'$ coupling (g^2_{Model}).

In this analysis, we consider several choices of the x_H and x_Φ to calculate the bounds in the $M'_Z - g'$ plane. These correspond to two scenarios: (i) x_H is negative and x_Φ is positive for which the results are shown in Fig. 12 and (ii) both x_H and x_Φ are positive and the corresponding constraints in the $M'_Z - g'$ plane are shown in Fig. 13. The interaction of the Z' with the fermions via the covariant derivative will depend on the x_H and x_ϕ values and is given by the Lagrangian,

$$-L_{\text{int}} \supset \overline{f_L}\gamma^\mu g' Q_x Z'_\mu f_L + \overline{f_R}\gamma^\mu g' Q'_x Z'_\mu f_R. \tag{7.2}$$

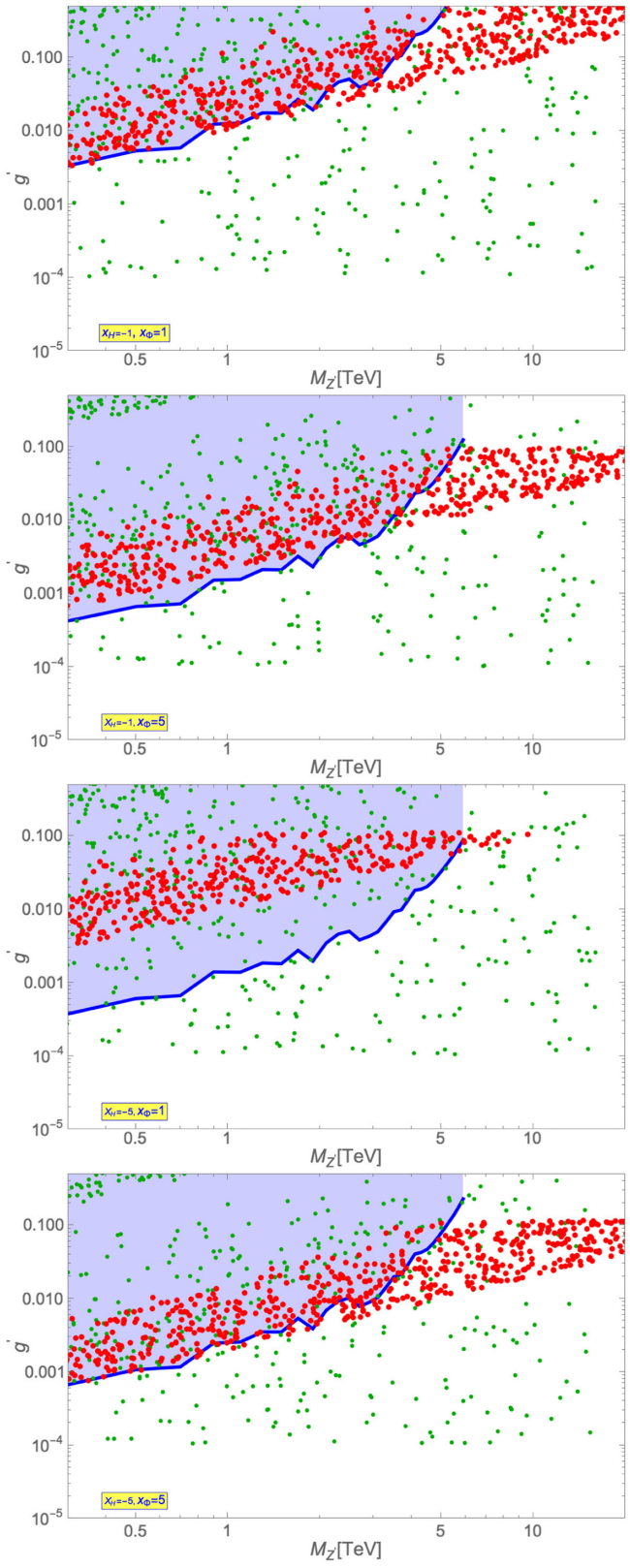

FIG. 12. Allowed parameter space combining the bounds obtained on g' as a function of M'_Z from vacuum stability and perturbativity (red dots), DM constraints (green dots), and collider (region below the blue solid line). The blue shaded regions are ruled out by the recent ATLAS search [40] at 139 fb^{-1} luminosity.

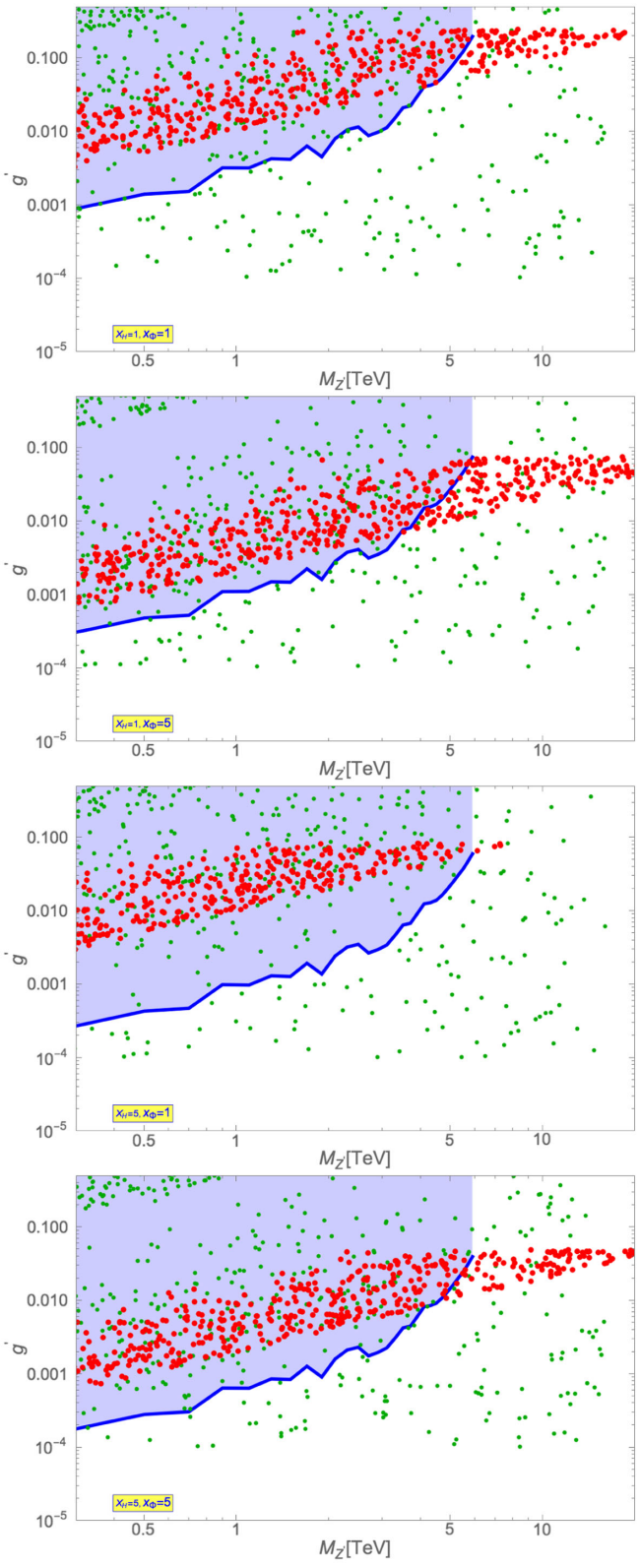

FIG. 13. Allowed parameter space combining the bounds obtained on g' as a function of M'_Z from vacuum stability and perturbativity (red dots), DM constraints (green dots), and collider (region below the blue solid line). The blue shaded regions are ruled out by the recent ATLAS search [40] at 139 fb^{-1} luminosity.

Here, f_L and f_R are the left-handed and right-handed fermions and Q_x and Q'_x are the corresponding charges under the $U(1)'$ gauge group. These charges are linear combinations of x_H and x_Φ and will appear in the C_V and C_A coefficients of the Z' interactions. The Z' interaction with the colored fermions will contain the color factor $N_c = 3$ in the interaction whereas $N_c = 1$ for the uncolored fermions. The bounds from the collider for various models are shown by the blue solid lines in Figs. 12 and 13. The blue shaded regions in these figures are ruled out by the current LHC data obtained from the ATLAS experiment [40] at 139 fb^{-1} luminosity.

In these figures, we have also given the bounds from vacuum stability, perturbativity, and relic density for purposes of comparison. For finding the regions that are allowed by vacuum stability and perturbativity, we have done a scanning in the following ranges of parameters:

$$g' \in [0.0001, 1.0], \qquad u \in [0.3, 100] \text{ TeV}$$
$$m_{h_2} \in [2.0, 16] \text{ TeV}, \qquad y^{33}_{NS} \in [0.2, 2.5], \tag{7.3}$$

with $\theta = 0.01$. For Y_ν and $(y_{NS})_{2\times 2}$, we have used BM-I from Table II and we have scaled y_{NS} according to the variation in u. The values of $M_{Z'}$ have been calculated using Eq. (5.2), and the allowed regions are shown by the red points in Figs. 12 and 13. It can be seen from these figures that the bulk of the parameter space allowed by vacuum stability lies in the region disfavored by the ATLAS results. Regions beyond $M_{Z'} > 5$ TeV that is not explored by ATLAS are seen to be allowed by vacuum stability and perturbativity constraints. Future ATLAS results will be able to explore this region.

Similarly, to find out the points that can give the correct DM relic density, we have performed a scanning of parameters in the ranges

$$g' \in [0.0001, 1.0], \; m_{Z'} \in [0.1, 16] \text{ TeV} \; m_{h_2} \in [2.0, 16] \text{ TeV},$$
$$y^{33}_{NS} \in [0.2, 2.5], \quad M_{\rm DM} \in [1.0, 10.0] \text{ TeV}. \tag{7.4}$$

Here also, we have fixed $\theta = 0.01$. The green dots in Figs. 12 and 13 correspond to the values that give the correct DM relic density. The constraints coming from this are seen to be less stringent than the combined constraints from vacuum stability, perturbativity, and ATLAS analysis.

VIII. CONCLUDING REMARKS

In this paper, we have studied the inverse seesaw model in a class of general $U(1)$ extensions of the SM. We have studied the parameter spaces in various planes that are allowed by vacuum stability and perturbativity as well as consistent with the low energy neutrino data. In addition, this model has a prospective DM candidate resulting from the stabilization of the third generations of the $SU(2)_L$ singlet neutral fermions using the odd parity under the discrete Z_2 symmetry. Comparing the Z' production and its decay into the dilepton mode at the LHC with the current ATLAS results, we find the bounds on the $U(1)'$ coupling constant with respect to the Z' mass. Finally, combining all the constraints, we obtain the resultant allowed parameter space which can be probed in the future experiments.

ACKNOWLEDGMENTS

This work of A. D. is supported by the Japan Society for the Promotion of Science Postdoctoral Fellowship for Research in Japan.

APPENDIX: ONE-LOOP RG EQUATIONS

$$\beta_{g_1} = \frac{1}{6}(41g_1^3 + g_1^2 g_{1p1}(78x_H + 64x_\Phi) + g_{11p}g_{1p1}(39g_{11p}x_H + 41g'x_H^2 + 32g_{11p}x_\Phi + 64g'x_Hx_\Phi + 66g'x_\Phi^2) + g_1(41g_{11p}^2 + g_{11p}g'(39x_H + 32x_\Phi) + g_{1p1}^2(41x_H^2 + 64x_Hx_\Phi + 66x_\Phi^2))), \tag{A1}$$

$$\beta_{g_2} = \frac{(-19g_2^3)}{6}, \tag{A2}$$

$$\beta g_3 = (-7g_3^3), \tag{A3}$$

$$\beta_{g'} = \frac{1}{6}(41g_{11p}^2 g' + g_{11p}(41g1g_{1p1} + (2g'^2 + g_{1p1}^2)(39x_H + 32x_\Phi)) + g'(g1g_{1p1}(39x_H + 32x_\Phi) + (g'^2 + g_{1p1}^2)(41x_H^2 + 64x_Hx_\Phi + 66x_\Phi^2))), \tag{A4}$$

$$\beta_{g_{1p1}} = \frac{1}{6}(41g_1^2 g_{1p1} + g1(41g_{11p}g' + (g'^2 + 2g_{1p1}^2)(39x_H + 32x_\Phi)) + g_{1p1}(g_{11p}g'(39x_H + 32x_\Phi) + (g'^2 + g_{1p1}^2)(41x_H^2 + 64x_Hx_\Phi + 66x_\Phi^2))), \tag{A5}$$

$$\beta_{g_{11p}} = \frac{1}{6}(g_1^2(41g_{11p} + 39g'x_H + 32g'x_\Phi) + g1g_{1p1}(39g_{11p}x_H + 41g'x_H^2 + 32g_{11p}x_\Phi + 64g'x_Hx_\Phi + 66g'x_\Phi^2) + g_{11p}(41g_{11p}^2 + g_{11p}g'(78x_H + 64x_\Phi) + g'^2(41x_H^2 + 64x_Hx_\Phi + 66x_\Phi^2))), \tag{A6}$$

$$\beta_{\lambda_1} = \frac{1}{8}(3g_1^4 + 6g_1^2g_{11p}^2 + 3g_{11p}^4 + 6g_1^2g_2^2 + 6g_{11p}^2g_2^2 + 9g_2^4 - 24g_1^2\lambda_1 - 24g_{11p}^2\lambda_1 - 72g_2^2\lambda_1 + 192\lambda_1^2 + 8\lambda_3^2 - 12g_1^2g_{11p}g'x_H - 12g_{11p}^3g'x_H - 12g_1^3g_{1p1}x_H - 12g_1g_{11p}^2g_{1p1}x_H - 12g_{11p}g'g_2^2x_H - 12g_1g_{1p1}g_2^2x_H + 48g_{11p}g'\lambda_1x_H + 48g_1g_{1p1}\lambda_1x_H + 6g_1^2g'^2x_H^2 + 18g_{11p}^2g'^2x_H^2 + 24g_1g_{11p}g'g_{1p1}x_H^2 + 18g_1^2g_{1p1}^2x_H^2 + 6g_{11p}^2g_{1p1}^2x_H^2 + 6g'^2g_2^2x_H^2 + 6g_{1p1}^2g_2^2x_H^2 - 24g'^2\lambda_1x_H^2 - 24g_{1p1}^2\lambda_1x_H^2 - 12g_{11p}g'^3x_H^3 - 12g_1g'^2g_{1p1}x_H^3 - 12g_{11p}g'g_{1p1}^2x_H^3 - 12g_1g_{1p1}^3x_H^3 + 3g'^4x_H^4 + 6g'^2g_{1p1}^2x_H^4 + 3g_{1p1}^4x_H^4 + 96\lambda_1y_t^2 + 32\lambda_1\mathrm{Tr}[Y_\nu Y_\nu^\dagger] - 48y_t^4 - 16\mathrm{Tr}[Y_\nu Y_\nu^\dagger Y_\nu Y_\nu^\dagger]), \tag{A7}$$

$$\beta_{\lambda_2} = (10\lambda_2^2 + \lambda_3^2 - 6g'^2\lambda_2x_\Phi^2 - 6g_{1p1}^2\lambda_2x_\Phi^2 + 3g'^4x_\Phi^4 + 2\lambda_2\mathrm{Tr}[y_{NS}y_{NS}^\dagger] - \mathrm{Tr}[y_{NS}y_{NS}^\dagger y_{NS}y_{NS}^\dagger]), \tag{A8}$$

$$\beta_{\lambda_3} = \frac{1}{2}(-3g_1^2\lambda_3 - 3g_{11p}^2\lambda_3 - 9g_2^2\lambda_3 + 24\lambda_1\lambda_3 + 16\lambda_2\lambda_3 + 8\lambda_3^2 + 6g_{11p}g'\lambda_3x_H + 6g1g_{1p1}\lambda_3x_H - 3g'^2\lambda_3x_H^2 - 3g_{1p1}^2\lambda_3x_H^2 + 6g_{11p}^2g'^2x_\Phi^2 - 12g'^2\lambda_3x_\Phi^2 - 12g_{1p1}^2\lambda_3x_\Phi^2 - 12g_{11p}g'^3x_Hx_\Phi^2 + 6g'^4x_H^2x_\Phi^2 + 12\lambda_3y_t^2 + 4\lambda_3\mathrm{Tr}[Y_\nu Y_\nu^\dagger] + 4\lambda_3\mathrm{Tr}[y_{NS}y_{NS}^\dagger] - 8\mathrm{Tr}[y_{NS}y_{NS}^\dagger Y_\nu Y_\nu^\dagger]), \tag{A9}$$

$$\beta_{y_t^{(1)}} = \frac{1}{12}(-((17g_1^2 + 17g_{11p}^2 + 27g_2^2 + 96g_3^2 + 34g_{11p}g'x_H + 34g1g_{1p1}x_H + 17g'^2x_H^2 + 17g_{1p1}^2x_H^2 + 20g_{11p}g'x_\Phi + 20g1g_{1p1}x_\Phi + 20g'^2x_Hx_\Phi + 20g_{1p1}^2x_Hx_\Phi + 8g'^2x_\Phi^2 + 8g_{1p1}^2x_\Phi^2 - 36y_t^2 - 12\mathrm{Tr}[Y_\nu Y_\nu^\dagger])y_t) + 18(y_t^3)), \tag{A10}$$

$$\beta_{y_{NS}^{(1)}} = ((-3(g'^2 + g_{1p1}^2)x_\Phi^2 + \mathrm{Tr}[y_{NS}y_{NS}^\dagger])y_{NS} + y_{NS}y_{NS}^\dagger y_{NS} + Y_\nu^T Y_\nu^* y_{NS}), \tag{A11}$$

$$\beta_{Y_\nu^{(1)}} = \frac{1}{4}(-((3g_1^2 + 3g_{11p}^2 + 9g_2^2 + 6g_{11p}g'x_H + 6g1g_{1p1}x_H + 3g'^2x_H^2 + 3g_{1p1}^2x_H^2 + 12g_{11p}g'x_\Phi + 12g1g_{1p1}x_\Phi + 12g'^2x_Hx_\Phi + 12g_{1p1}^2x_Hx_\Phi + 24g'^2x_\Phi^2 + 24g_{1p1}^2x_\Phi^2 - 12y_t^2 - 4\mathrm{Tr}[Y_\nu Y_\nu^\dagger])Y\nu) + 2(3Y\nu Y_\nu^\dagger Y_\nu + Y_\nu y_{NS}^* y_{NS}^T)). \tag{A12}$$

[1] S. Chatrchyan *et al.* (CMS Collaboration), Observation of a new boson at a mass of 125 GeV with the CMS experiment at the LHC, Phys. Lett. B **716**, 30 (2012).

[2] G. Aad *et al.* (ATLAS Collaboration), Observation of a new particle in the search for the Standard Model Higgs boson with the ATLAS detector at the LHC, Phys. Lett. B **716**, 1 (2012).

[3] P. Minkowski, mu → e gamma at a rate of one out of 1-billion muon decays?, Phys. Lett. **67B**, 421 (1977).

[4] P. Van Nieuwenhuizenand D. Z. Freedman, *Supergravity: Proceedings, Workshop at Stony Brook* (North-Holland, Amsterdam, Netherlands, 1979), p. 341.

[5] *Workshop on Unified Theory and Baryon Number in the Universe*, edited by O. Sawada, A. Sugamoto, and K. E K. Tsukuba (Natl.Lab.High Energy Phys., Tsukuba, Japan, 1979), p. 109.

[6] R. N. Mohapatra and G. Senjanovic, Neutrino Mass and Spontaneous Parity Violation, Phys. Rev. Lett. **44**, 912 (1980).

[7] S. M. Boucenna, S. Morisi, and J. W. F. Valle, The low-scale approach to neutrino masses, Adv. High Energy Phys. **2014**, 1 (2014).

[8] F. F. Deppisch, P. S. Bhupal Dev, and A. Pilaftsis, Neutrinos and collider physics, New J. Phys. **17**, 075019 (2015).

[9] Y. Cai, T. Han, T. Li, and R. Ruiz, Lepton number violation: Seesaw models and their collider tests, Front. Phys. **6**, 40 (2018).

[10] A. Das, Searching for the minimal seesaw models at the LHC and beyond, Adv. High Energy Phys. **2018**, 9785318 (2018).

[11] R. Mohapatra and J. Valle, Neutrino mass and baryon number nonconservation in superstring models, Phys. Rev. D **34**, 1642 (1986).
[12] A. Datta, A. Elsayed, S. Khalil, and A. Moursy, Higgs vacuum stability in the $B-L$ extended standard model, Phys. Rev. D **88**, 053011 (2013).
[13] S. Iso, N. Okada, and Y. Orikasa, The minimal $B-L$ model naturally realized at TeV scale, Phys. Rev. D **80**, 115007 (2009).
[14] S. Iso, N. Okada, and Y. Orikasa, Classically conformal $B-L$ extended Standard Model, Phys. Lett. B **676**, 81 (2009).
[15] S. Iso and Y. Orikasa, TeV Scale $B-L$ model with a flat Higgs potential at the Planck scale: In view of the hierarchy problem, Prog. Theor. Exp. Phys. (**2013**), 023B08.
[16] J. Chakrabortty, P. Konar, and T. Mondal, Constraining a class of BL extended models from vacuum stability and perturbativity, Phys. Rev. D **89**, 056014 (2014).
[17] C. Coriano, L. Delle Rose, and C. Marzo, Vacuum stability in $U(1)$-prime extensions of the standard model with TeV scale right handed neutrinos, Phys. Lett. B **738**, 13 (2014).
[18] C. Coriano, L. Delle Rose, and C. Marzo, Constraints on Abelian extensions of the Standard Model from two-loop vacuum stability and $U(1)_{B-L}$, J. High Energy Phys. 02 (2016) 135.
[19] A. Das, N. Okada, and N. Papapietro, Electroweak vacuum stability in classically conformal $B-L$ extension of the Standard Model, Eur. Phys. J. C **77**, 122 (2017).
[20] E. Accomando, C. Coriano, L. Delle Rose, J. Fiaschi, C. Marzo, and S. Moretti, Z, Higgses and heavy neutrinos in $U(1)$ models: From the LHC to the GUT scale, J. High Energy Phys. 07 (2016) 086.
[21] S. Oda, N. Okada, and D.-s. Takahashi, Classically conformal $U(1)$ extended standard model and Higgs vacuum stability, Phys. Rev. D **92**, 015026 (2015).
[22] A. Das, S. Oda, N. Okada, and D.-s. Takahashi, Classically conformal $U(1)$ extended standard model, electroweak vacuum stability, and LHC Run-2 bounds, Phys. Rev. D **93**, 115038 (2016).
[23] S. Alekhin, A. Djouadi, and S. Moch, The top quark and Higgs boson masses and the stability of the electroweak vacuum, Phys. Lett. B **716**, 214 (2012).
[24] D. Buttazzo, G. Degrassi, P. P. Giardino, G. F. Giudice, F. Sala, A. Salvio, and A. Strumia, Investigating the near-criticality of the Higgs boson, J. High Energy Phys. 12 (2013) 089.
[25] P. A. R. Ade *et al.* (Planck Collaboration), Planck 2015 results. XIII. Cosmological parameters, Astron. Astrophys. **594**, A13 (2016).
[26] T. Basak and T. Mondal, Constraining minimal $U(1)_{B-L}$ model from dark matter observations, Phys. Rev. D **89**, 063527 (2014).
[27] S. Oda, N. Okada, and D.-s. Takahashi, Right-handed neutrino dark matter in the classically conformal $U(1)$ extended standard model, Phys. Rev. D **96**, 095032 (2017).
[28] W. Rodejohann and C. E. Yaguna, Scalar dark matter in the BL model, J. Cosmol. Astropart. Phys. 12 (2015) 032.
[29] J. Cao, L. Feng, X. Guo, L. Shang, F. Wang, and P. Wu, Scalar dark matter interpretation of the DAMPE data with $U(1)$ gauge interactions, Phys. Rev. D **97**, 095011 (2018).
[30] S. Singirala, R. Mohanta, and S. Patra, Singlet scalar dark matter in $U(1)_{B-L}$ models without right-handed neutrinos, Eur. Phys. J. Plus **133**, 477 (2018).
[31] D. A. Camargo, M. D. Campos, T. B. de Melo, and F. S. Queiroz, A two Higgs doublet model for dark matter and neutrino masses, Phys. Lett. B **795**, 319 (2019).
[32] P. Langacker, Grand unified theories and proton decay, Phys. Rep. **72**, 185 (1981).
[33] J. L. Hewett and T. G. Rizzo, Low-energy phenomenology of superstring inspired E(6) models, Phys. Rep. **183**, 193 (1989).
[34] L. Basso, A. Belyaev, S. Moretti, and C. H. Shepherd-Themistocleous, Phenomenology of the minimal $B-L$ extension of the Standard model: Z' and neutrinos, Phys. Rev. D **80**, 055030 (2009).
[35] M. Lindner, M. Platscher, and F. S. Queiroz, A call for new physics: The muon anomalous magnetic moment and lepton flavor violation, Phys. Rep. **731**, 1 (2018).
[36] A. Ekstedt, R. Enberg, G. Ingelman, J. Lfgren, and T. Mandal, Constraining minimal anomaly free $U(1)$ extensions of the Standard Model, J. High Energy Phys. 11 (2016) 071.
[37] E. Accomando, L. Delle Rose, S. Moretti, E. Olaiya, and C. H. Shepherd-Themistocleous, Extra Higgs boson and Z as portals to signatures of heavy neutrinos at the LHC, J. High Energy Phys. 02 (2018) 109.
[38] M. Aaboud *et al.* (ATLAS Collaboration), Search for high-mass new phenomena in the dilepton final state using proton-proton collisions at $\sqrt{s}=13$ TeV with the ATLAS detector, Phys. Lett. B **761**, 372 (2016).
[39] V. Khachatryan *et al.* (CMS Collaboration), Search for narrow resonances in dilepton mass spectra in proton-proton collisions at $\sqrt{s}=13$ TeV and combination with 8 TeV data, Phys. Lett. B **768**, 57 (2017).
[40] G. Aad *et al.* (ATLAS Collaboration), Search for high-mass dilepton resonances using 139 fb^{-1} of pp collision data collected at $\sqrt{s}=13$ TeV with the ATLAS detector, Phys. Lett. B **796**, 68 (2019).
[41] K. Kannike, Vacuum stability conditions from copositivity criteria, Eur. Phys. J. C **72**, 2093 (2012).
[42] J. Chakrabortty, P. Konar, and T. Mondal, Copositive criteria and boundedness of the scalar potential, Phys. Rev. D **89**, 095008 (2014).
[43] H. Huffel and G. Pocsik, Unitarity bounds on Higgs boson masses in the Weinberg-Salam model with two Higgs doublets, Z. Phys. C **8**, 13 (1981).
[44] M. Duerr, F. Kahlhoefer, K. Schmidt-Hoberg, T. Schwetz, and S. Vogl, How to save the WIMP: Global analysis of a dark matter model with two s-channel mediators, J. High Energy Phys. 09 (2016) 042.
[45] W. T. V. W. H. Press, S. A. Teukolsky, and B. P. Flannery, *Numerical Recipes in Fortran 90*, 2nd ed. (Cambridge University Press, Cambridge, United Kingdom, 1996).
[46] N. Aghanim *et al.* (Planck Collaboration), Planck 2018 results. VI. Cosmological parameters, arXiv:1807.06209.
[47] I. Esteban, M. C. Gonzalez-Garcia, A. Hernandez-Cabezudo, M. Maltoni, and T. Schwetz, Global analysis of three-flavour neutrino oscillations: Synergies and tensions in the determination of $\theta_2 3$, $\delta_C P$, and the mass ordering, J. High Energy Phys. 01, 109, (2019).

[48] I. Esteban, M. C. Gonzalez-Garcia, M. Maltoni, I. Martinez-Soler, and T. Schwetz, Updated fit to three neutrino mixing: Exploring the accelerator-reactor complementarity, J. High Energy Phys. 01 (2017) 087.

[49] F. Capozzi, E. Lisi, A. Marrone, D. Montanino, and A. Palazzo, Neutrino masses and mixings: Status of known and unknown 3ν parameters, Nucl. Phys. **B908**, 218 (2016).

[50] S. Antusch and O. Fischer, Probing the nonunitarity of the leptonic mixing matrix at the CEPC, Int. J. Mod. Phys. A **31**, 1644006 (2016).

[51] A. M. Baldini *et al.* (MEG Collaboration), Search for the lepton flavour violating decay $\mu^+ \to e^+\gamma$ with the full dataset of the MEG experiment, Eur. Phys. J. C **76**, 434 (2016).

[52] R. Coy and M. Frigerio, Effective approach to lepton observables: The seesaw case, Phys. Rev. D **99**, 095040 (2019).

[53] W. H. Bertl *et al.* (SINDRUM II Collaboration), A search for muon to electron conversion in muonic gold, Eur. Phys. J. C **47**, 337 (2006).

[54] A. Sirlin and R. Zucchini, Dependence of the quartic coupling H(m) on M(H) and the possible onset of new physics in the Higgs sector of the standard model, Nucl. Phys. **B266**, 389 (1986).

[55] K. Melnikov and T. V. Ritbergen, The three loop relation between the MS-bar and the pole quark masses, Phys. Lett. B **482**, 99 (2000).

[56] M. Holthausen, K. S. Lim, and M. Lindner, Planck scale boundary conditions and the Higgs mass, J. High Energy Phys. 02 (2012) 037.

[57] F. Staub, SARAH 4: A tool for (not only SUSY) model builders, Comput. Phys. Commun. **185**, 1773 (2014).

[58] G. Blanger, F. Boudjema, A. Pukhov, and A. Semenov, micrOMEGAs4.1: Two dark matter candidates, Comput. Phys. Commun. **192**, 322 (2015).

[59] G. Belanger, F. Boudjema, A. Pukhov, and A. Semenov, $micrOMEGAs_3$: A program for calculating dark matter observables, Comput. Phys. Commun. **185**, 960 (2014).

[60] X. Cui *et al.* (PandaX-II Collaboration), Dark Matter Results from 54-Ton-Day Exposure of PandaX-II Experiment, Phys. Rev. Lett. **119**, 181302 (2017).

[61] E. Aprile *et al.* (XENON Collaboration), First Dark Matter Search Results from the XENON1T Experiment, Phys. Rev. Lett. **119**, 181301 (2017).

[62] P. Langacker, The physics of heavy Z' gauge bosons, Rev. Mod. Phys. **81**, 1199 (2009).